INSTITUTE OF PHYSICS PUBLISHING PLASMA PHYSICS AND CONTROLLED FUSION

Plasma Phys. Control. Fusion **43** (2001) 825–837 www.iop.org/Journals/pp PII: S0741-3335(01)23330-2

Zonal flow and streamer generation in drift turbulence

G Manfredi[1], **C M Roach**[2] **and R O Dendy**[2]

[1] Laboratoire de Physique des Milieux Ionisés, Université Henri Poincaré, BP 239, 54506 Vandoeuvre-les-Nancy, France
[2] Euratom/UKAEA Fusion Association, Culham Science Centre, Abingdon, Oxfordshire, UK

Received 26 March 2001

Abstract

The relative importance of poloidally extended zonal flows ($k_\theta = 0,\ k_r \neq 0$) and radially extended streamers ($k_\theta \neq 0,\ k_r = 0$) in regulating drift turbulent energy transport is a central question in tokamak physics. Both forms of nonlinear structure can be described within the framework of the Hasegawa–Mima equation, as extended by Smolyakov *et al* (Smolyakov A I, Diamond P H and Malkov M 2000 *Phys. Rev. Lett.* **84** 491), although streamers have not previously been analysed in this context. Here we present results obtained by comparing analytical weak-turbulence calculations with numerical simulations using a spectral code. The analytical results are obtained with a four-wave model, incorporating a drift wave ($\boldsymbol{k}_2$) coupled to both sidebands ($\boldsymbol{k}_2 \pm \boldsymbol{k}_1$) by a zonal flow or streamer ($\boldsymbol{k}_1$). Fully nonlinear studies of this four-wave system have been carried out, and we find that analytical expressions derived from wave coupling models provide a good guide to the spectral code results. Instability conditions are found and growth rates computed, showing that zonal flows are more unstable than streamers, at least at this level of description. Typically, we find that the streamer growth rate is lower than that of the zonal flow by a factor of order $\rho_s k_1$. Insofar as our Hasegawa–Mima model contains many of the core physics elements of more sophisticated approaches, these results are of wider importance to the numerical modelling of drift turbulence in tokamaks.

1. Introduction

Drift waves play an important role in the physics of strongly magnetized plasmas. When unstable, such as in the presence of steep enough temperature gradients, they can give rise to fully developed 'drift' turbulence, which is presumably responsible for the anomalous transport rates observed in present tokamaks. Various models of increasing complexity and realism have been proposed in the past decades to study the (possibly turbulent) dynamics of drift waves, including both gyrokinetic and (gyro)fluid models [1–7], and realistic three-dimensional simulations in toroidal geometry are now available. These simulations have shown that 'zonal flows' are a crucial factor in regulating the nonlinear evolution of drift-wave instabilities, such as the ion temperature gradient (ITG) instability, and consequently the level of turbulent transport. The generally accepted argument is that the radial dependence of the

0741-3335/01/060825+13$30.00

zonal flow generates a poloidal $\boldsymbol{E} \times \boldsymbol{B}$ sheared rotation, which depresses anomalous transport by reducing the radial correlation length.

Zonal flows are defined as modes that only depend on the radial coordinate r, and generally vary on time scales slower than those corresponding to drift waves. We note that this definition includes both large-scale flux-surface-averaged flows (satisfying $\rho_s k_r \ll 1$ with scale length possibly approaching the machine size, where $\rho_s = \sqrt{T_e m_i}/eB$ is the ion thermal Larmor radius at the electron temperature) and small-scale modes (with scale length comparable to the ion Larmor radius, $\rho_s k_r \simeq 1$), provided they have no poloidal or toroidal dependence. In the rest of this paper, the term zonal flow will generally be used to refer to the large scale structures, although our formalism is equally appropriate for dealing with small-scale structures.

On the other hand, zonal flows have long been observed in numerical simulations of rotating neutral fluids, and have been invoked to explain the striped appearance of the atmosphere of the giant planets. Indeed, mathematical models for rotating fluids are very similar to models developed for the study of drift waves in magnetized plasmas. Perhaps the simplest such plasma model is the Hasegawa–Mima equation [8], which is almost identical in structure to the Charney equation [9], describing two-dimensional fluid turbulence in a rotating frame. It has been shown that the interplay of linear drift-wave propagation with nonlinear coupling can give rise to strongly anisotropic spectra, dominated by zonal flows [10]. Note, however, that these zonal flows are small-scale radial modes, and not large-scale structures such as those considered in the rest of this paper.

Recently, several theoretical models have been proposed in order to explain the emergence of zonal flows in tokamak plasmas. Smolyakov, Diamond and co-workers have suggested [11, 12] that zonal flows can be generated spontaneously in the presence of a bath of small-scale drift waves. They indicated two possible regimes, corresponding to two different types of instability: (a) when the drift wave spectrum is narrow, the instability is of the modulational type [12]; (b) when the spectrum is broad and almost continuous, integration over all wavenumbers can yield a resonant instability [11].

The former case is investigated analytically and numerically in the present paper. It is first shown (section 3) that the results obtained in [12] can be readily derived using a relatively simple four-wave model [13, 14], which describes the evolution of the pump drift wave, its two sidebands, and a large-scale wave (zonal flow). An analogous treatment is then extended to the case where the large-scale wave is a *streamer*, which has not been previously analysed. A streamer is defined here as a radially elongated large-scale mode that does not depend on the radial coordinate ($k_r = 0$), and is slowly varying in the poloidal direction ($\rho_s k_\theta \ll 1$). The model exhibits an instability for the streamer or zonal flow, which eventually saturates by depletion of the pump wave. Numerical simulations of the instability, presented in section 4, yield a growth rate that is in agreement with the analytical calculations. The relevance of these results to the physics of tokamak plasmas is discussed in the final section.

2. Model

The model used in this paper is the one adopted by Smolyakov *et al* [11, 12] to describe the dynamics of drift waves in the poloidal plane in a sheared magnetic field. It is essentially a Hasegawa–Mima (HM) equation [8], and is based on the same assumptions of cold ions, $T_i \ll T_e$, ($T_{i(e)}$ being the ion (electron) temperature), with negligible inertia parallel to the magnetic field. The quasineutrality condition $n_i = n_e$ is satisfied, where $n_{i(e)}$ is the ion (electron) density; the electrons are assumed to have an immediate adiabatic response, with Boltzmann distribution. For global flows, however, the density fluctuation does not depend on the averaged (on a flux surface) part of the electrostatic potential $\bar{\phi}$. In order to relate the

density fluctuation to the potential, one should therefore write [4]

$$\frac{n_{\mathrm{i,e}} - n_0}{n_0} = \frac{e}{T_{\mathrm{e}}}(\phi - \bar{\phi}) \tag{1}$$

where $n_0(y)$ is the equilibrium density and $\phi(x, y, t)$ the electrostatic potential. The latter can be represented as the sum of a flux-surface averaged value $\bar{\phi}$ and a contribution $\tilde{\phi}$ which varies on a flux surface. As we use two-dimensional slab geometry, with x the poloidal and y the radial coordinate (this convention is that used in geophysical fluid dynamics, but not the one commonly used in fusion theory), one simply has that $\bar{\phi} = \frac{1}{L}\int_0^L \phi \, \mathrm{d}x$ (where L is the slab size in the poloidal direction). Note that equation (1) means that the flux-averaged part of the electron density does not respond adiabatically. This is because the electrons are thermalized along the magnetic field lines (and therefore on a flux surface), but not across flux surfaces.

With these assumptions, the relevant model is written as

$$\frac{\partial}{\partial t}(\tilde{\phi} - \rho_{\mathrm{s}}^2 \nabla_\perp^2 \phi) + (\boldsymbol{v}_0 + \tilde{\boldsymbol{v}}_{\mathrm{E}}) \cdot \boldsymbol{\nabla}(\tilde{\phi} - \rho_{\mathrm{s}}^2 \nabla_\perp^2 \phi) + \boldsymbol{v} \cdot \boldsymbol{\nabla}\tilde{\phi} = 0 \tag{2}$$

where $\boldsymbol{v}_0$ and $\tilde{\boldsymbol{v}}_{\mathrm{E}}$ are the electric drift velocities arising from $\bar{\phi}$ and $\tilde{\phi}$, respectively

$$\boldsymbol{v}_0 = \frac{\hat{z} \times \boldsymbol{\nabla}\bar{\phi}}{B} \qquad \text{and} \qquad \tilde{\boldsymbol{v}}_{\mathrm{E}} = \frac{\hat{z} \times \boldsymbol{\nabla}\tilde{\phi}}{B}.$$

Here $\boldsymbol{v} = \hat{x} T_{\mathrm{e}}/(eBL_{\mathrm{n}})$ is the electron diamagnetic drift velocity, and L_{n} is the characteristic length scale of the plasma inhomogeneity. Boundary conditions are taken to be periodic in both directions, with spatial period equal to L (which represents a macroscopic length scale, such as the minor radius, in tokamak configuration). Notice that the standard Hasegawa–Mima equation can be recovered by neglecting mean flows, i.e. by letting $\bar{\phi} = 0$ so that $\phi \to \tilde{\phi}$ everywhere in equation (2).

Equation (2) is the model used throughout this paper for the study of zonal flows and streamers, and is identical to equation (1) of [11]. We stress that this equation includes several essential ingredients that appear in more sophisticated models of drift turbulence and transport. In particular, it has been shown that the prescription of equation (1) is responsible for the appearance of large-scale average flows in ITG simulations [4]. One should bear in mind, however, that this is an approximate model, which sheds light on the evolution of zonal flows and streamers, but necessarily employs some simplified physics. In particular, the model does not include a temperature gradient, which is the main instability drive in large-scale transport codes. Moreover, magnetic shear is not included and, due to the periodic boundary conditions, the modes are not radially bounded.

3. Weak turbulence analysis: the four-wave problem

As we shall be mainly interested in mode couplings, it is useful to expand the total potential ϕ in a Fourier series

$$\phi(\boldsymbol{r}, t) = \sum_j \phi_j(t) \exp(\mathrm{i}\boldsymbol{k}_j \cdot \boldsymbol{r}). \tag{3}$$

The requirement that $\bar{\phi}$ and $\tilde{\phi}$ must be real imposes the following constraints on the complex Fourier amplitudes:

$$\phi_{-j} = \phi_j^* \tag{4}$$

with $\boldsymbol{k}_{-j} = -\boldsymbol{k}_j$.

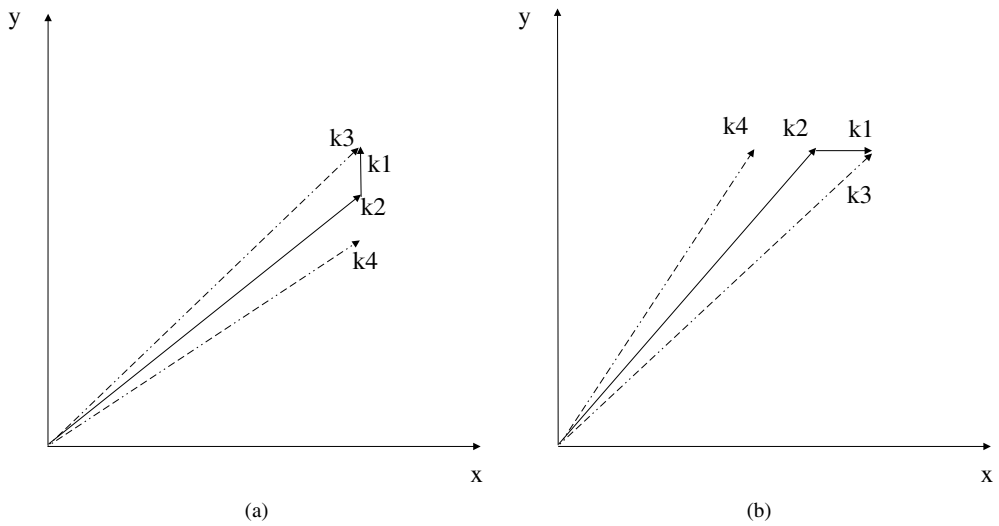

Figure 1. Slab geometry with the flux surfaces parallel to the x-axis, and the magnetic field aligned in the z direction. The arrows denote the wavevectors for the four wave problems: (a) corresponds to the generation of zonal flows parallel to flux surfaces, and (b) shows the generation of flows across flux surfaces in the radial direction (streamers).

With this representation, equation (2) can be written as

$$\frac{\partial \phi_j}{\partial t} + \mathrm{i}\Omega_j \phi_j = \sum_{m,n} \Lambda^j_{m,n} \phi_n \phi_m \tag{5}$$

where the sum is extended over all wavenumbers such that $\boldsymbol{k}_j = \boldsymbol{k}_m + \boldsymbol{k}_n$. The $\Lambda^j_{m,n}$ are appropriate nonlinear coupling coefficients, and

$$\Omega_j = \frac{\boldsymbol{v} \cdot \boldsymbol{k}_j}{1 + \rho_s^2 k_j^2} \tag{6}$$

are the linear drift frequencies. Notice that for the zonal flow $\Omega_1 = 0$, as the corresponding wavevector is perpendicular to the flux surface.

Finally, we point out that the generalized HM model admits two quadratic invariants (just like the original HM equation). These are the energy

$$E = \sum_j \rho_s^2 k_j^2 |\bar{\phi}_j|^2 + \sum_j (1 + \rho_s^2 k_j^2) |\tilde{\phi}_j|^2 \tag{7}$$

and the generalized enstrophy

$$Z = \sum_j \rho_s^4 k_j^4 |\bar{\phi}_j|^2 + \sum_j (1 + \rho_s^2 k_j^2)^2 |\tilde{\phi}_j|^2. \tag{8}$$

These invariants are of considerable importance in the statistical theory of the HM model, and will be used later on in order to obtain information about the nonlinear saturation of the instability.

3.1. Zonal flow generation

A weak turbulence analysis of the generalized HM system can be obtained in the special case where only four nonlinearly coupled modes are present. We consider the situation where a

large amplitude pump wave with wavevector $\boldsymbol{k}_2$ is present, with two much smaller sidebands ($\boldsymbol{k}_3$ and $\boldsymbol{k}_4$) and a small amplitude zonal flow with wavevector $\boldsymbol{k}_1$ perpendicular to the flux surfaces (i.e. $k_{1x} = 0$). The wavevectors must be chosen such that the following conditions are satisfied

$$\boldsymbol{k}_4 + \boldsymbol{k}_1 = \boldsymbol{k}_2 \qquad \boldsymbol{k}_3 - \boldsymbol{k}_1 = \boldsymbol{k}_2.$$

In addition, the wavenumber of the zonal flow is much smaller than the other three ($k_1 \ll k_{2,3,4}$). The wavevectors and geometry of the system are illustrated in figure 1(a). In order to perform a linear analysis of the four-wave system, we must specify that $\phi_2 \gg \phi_4, \phi_3, \phi_1$, and include Fourier amplitudes for wavevectors $-\boldsymbol{k}_1$, $-\boldsymbol{k}_2$, $-\boldsymbol{k}_3$ and $-\boldsymbol{k}_4$, noting the constraint from equation (4).

With this restricted set of Fourier amplitudes, linearizing equation (2) (i.e. assuming $\phi_2 \gg \phi_4, \phi_3, \phi_1$) gives the following set of four coupled equations for the amplitudes $\phi_1(t)$, $\phi_2(t)$, $\phi_3(t)$ and $\phi_4(t)$:

$$k_1^2\rho_s^2\dot{\phi}_1 = A\rho_s^2[\phi_3\phi_2^*(k_2^2 - k_3^2) + \phi_2\phi_4^*(k_4^2 - k_2^2)] \tag{9}$$

$$(1 + \rho_s^2k_2^2)\dot{\phi}_2 + \mathrm{i}\boldsymbol{v}\cdot\boldsymbol{k}_2\phi_2 = 0 \tag{10}$$

$$(1 + \rho_s^2k_3^2)\dot{\phi}_3 + \mathrm{i}\boldsymbol{v}\cdot\boldsymbol{k}_3\phi_3 = -A\phi_1\phi_2(1 + k_2^2\rho_s^2 - k_1^2\rho_s^2) \tag{11}$$

$$(1 + \rho_s^2k_4^2)\dot{\phi}_4 + \mathrm{i}\boldsymbol{v}\cdot\boldsymbol{k}_4\phi_4 = A\phi_1^*\phi_2(1 + k_2^2\rho_s^2 - k_1^2\rho_s^2) \tag{12}$$

where $A = \hat{\boldsymbol{z}}\cdot\boldsymbol{k}_2\times\boldsymbol{k}_1/B = \hat{\boldsymbol{z}}\cdot\boldsymbol{k}_3\times\boldsymbol{k}_1/B = \hat{\boldsymbol{z}}\cdot\boldsymbol{k}_4\times\boldsymbol{k}_1/B = \hat{\boldsymbol{z}}\cdot\boldsymbol{k}_4\times\boldsymbol{k}_2/B = \hat{\boldsymbol{z}}\cdot\boldsymbol{k}_2\times\boldsymbol{k}_3/B$, and a dot denotes differentiation with respect to time. Simple manipulation of this system of equations shows that $\phi_1(t)$ must be a solution of the following third-order differential equation with respect to t

$$\dddot{\phi}_1 - \mathrm{i}(\Delta_{23} + \Delta_{42})\ddot{\phi}_1 - \left[A^2|\phi_2|^2\frac{\alpha}{k_1^2} + \Delta_{42}\Delta_{23}\right]\dot{\phi}_1 = 0 \tag{13}$$

where

$$\alpha = (1 + k_2^2\rho_s^2 - k_1^2\rho_s^2)\left(\frac{k_4^2 - k_2^2}{1 + k_4^2\rho_s^2} - \frac{k_2^2 - k_3^2}{1 + k_3^2\rho_s^2}\right) \tag{14}$$

and

$$\Delta_{23} = \Omega_2 - \Omega_3 \qquad \text{and} \qquad \Delta_{42} = \Omega_4 - \Omega_2. \tag{15}$$

The Ω are defined in equation (6).

Seeking solutions to equation (13) of the form $\phi_1(t) = \phi_1 e^{\lambda t}$ gives a quadratic equation for λ, which has the following solution

$$\lambda = \mathrm{i}\frac{\Delta_{23} + \Delta_{42}}{2} \pm \sqrt{A^2|\phi_2|^2\frac{\alpha}{k_1^2} - \frac{(\Delta_{23} - \Delta_{42})^2}{4}}. \tag{16}$$

There is instability when λ has a nonzero real part, which occurs if

$$A^2|\phi_2|^2\frac{\alpha}{k_1^2} > \frac{(\Delta_{23} - \Delta_{42})^2}{4}. \tag{17}$$

Otherwise both solutions are oscillatory.

The linear growth rate γ_Z of the unstable mode is given by the real part of λ:

$$\gamma_Z = \sqrt{A^2|\phi_2|^2\frac{\alpha}{k_1^2} - \frac{(\Delta_{23} - \Delta_{42})^2}{4}}. \tag{18}$$

The weak turbulence dispersion relation and threshold emerging from equation (13) have the standard form for the modulational instability–compare, for example, equations (2.27)–(2.29) of [15]. Physically, the nonlinearities of equation (2) manifest themselves in two ways in the four-wave weak turbulence approximation, as follows. The pump wave creates a ponderomotive force that can drive the zonal flow; in return, the zonal flow itself perturbs the dispersive properties of both the pump wave and the sideband waves that couple the pump to the zonal flow. Therefore, the previous results shed light on the threshold and initial growth of the resulting instability. To advance further into the nonlinear regime, we require numerical results from the spectral code presented in section 4.

Smolyakov *et al* [12] have presented a more elaborate analysis of this weak turbulence problem, by self-consistently solving the kinetic equation for wave packets and using the adiabatic action invariant. They have presented results in the limit where $k_1\rho_s \ll 1$ and where terms proportional to $(k_2^2\rho_s^2)^2$ can be neglected. In this limit, the term $(\Delta_{23}-\Delta_{42})^2$ in equation (18) is much smaller than the other term, and we find that our growth rate reduces to

$$\gamma_Z = \frac{\sqrt{2}|\phi_2|k_1k_{2x}}{B(1+k_2^2\rho_s^2)^{\frac{1}{2}}}\sqrt{1+\rho_s^2(k_2^2-4k_{2y}^2)}. \tag{19}$$

Using the notation of [12] with $k_1 \to q, k_2 \to k_\perp, x \to \theta, y \to r$, and $(1+k_2^2\rho_s^2)|\phi_2|/B\rho_s c_s \to N_0^{\frac{1}{2}}$, this becomes

$$\gamma_Z = \frac{\sqrt{2}N_0^{\frac{1}{2}}\rho_s c_s q k_{2\theta}}{(1+\rho_s^2k_\perp^2)^{\frac{3}{2}}}\sqrt{1+\rho_s^2(k_\perp^2-4k_{2r}^2)}. \tag{20}$$

where $c_s = \sqrt{T_e/m_i}$ is the sound speed. Equation (20) appears to differ by a factor of $\sqrt{2}$ from the result in equation (15) of [12], which was obtained using quite different methods.

3.2. Streamers

Here we consider a similar four-wave problem, but with sidebands ($\phi_{3,4}$) to the pump wave (ϕ_2) excited with a poloidal displacement, giving rise to the growth of a long wavelength streamer (ϕ_1) as depicted in figure 1(b). The streamer is a mode with zero radial wavenumber (i.e. $k_{1y}=0$), therefore extending over many flux surfaces.

With this restricted set of Fourier amplitudes, linearizing equation (2) (assuming $\phi_2 \gg \phi_4, \phi_3, \phi_1$) gives the following set of four coupled equations for the amplitudes $\phi_1(t)$, $\phi_2(t)$, $\phi_3(t)$ and $\phi_4(t)$:

$$(1+k_1^2\rho_s^2)\dot{\phi}_1 + \mathrm{i}\boldsymbol{v}\cdot\boldsymbol{k}_1\phi_1 = -A'\rho_s^2(\phi_3\phi_2^*(k_2^2-k_3^2)+\phi_2\phi_4^*(k_4^2-k_2^2)) \tag{21}$$

$$(1+\rho_s^2k_2^2)\dot{\phi}_2 + \mathrm{i}\boldsymbol{v}\cdot\boldsymbol{k}_2\phi_2 = 0 \tag{22}$$

$$(1+\rho_s^2k_3^2)\dot{\phi}_3 + \mathrm{i}\boldsymbol{v}\cdot\boldsymbol{k}_3\phi_3 = A'\phi_1\phi_2(k_2^2\rho_s^2-k_1^2\rho_s^2) \tag{23}$$

$$(1+\rho_s^2k_4^2)\dot{\phi}_4 + \mathrm{i}\boldsymbol{v}\cdot\boldsymbol{k}_4\phi_4 = -A'\phi_1^*\phi_2(k_2^2\rho_s^2-k_1^2\rho_s^2) \tag{24}$$

where $A' = \hat{\boldsymbol{z}}\cdot\boldsymbol{k}_1\times\boldsymbol{k}_2/B = \hat{\boldsymbol{z}}\cdot\boldsymbol{k}_1\times\boldsymbol{k}_3/B = \hat{\boldsymbol{z}}\cdot\boldsymbol{k}_1\times\boldsymbol{k}_4/B = \hat{\boldsymbol{z}}\cdot\boldsymbol{k}_2\times\boldsymbol{k}_4/B = \hat{\boldsymbol{z}}\cdot\boldsymbol{k}_3\times\boldsymbol{k}_2/B$. Note that A' has a different definition to the parameter A defined in section 3.1, so that both A and A' are positive numbers. Simple manipulation of this system of equations shows that $\phi_1(t)$ must be a solution of the following third-order differential equation with respect to t:

$$\dddot{\phi}_1 - \mathrm{i}\,(\Delta_{23}+\Delta_{42}-\Delta_1)\,\ddot{\phi}_1 + \left[\Delta_1\,(\Delta_{42}+\Delta_{23}) - \frac{A'^2|\phi_2|^2\Gamma\rho_s^4}{1+k_1^2\rho_s^2} - \Delta_{42}\Delta_{23}\right]\dot{\phi}_1$$
$$+\mathrm{i}\left(\frac{A'^2\Gamma|\phi_2|^2\rho_s^4\Delta_{42}}{1+k_1^2\rho_s^2} - \frac{A'^2\Delta|\phi_2|^2\rho_s^4(k_2^2-k_4^2)(k_1^2-k_2^2)}{(1+k_1^2\rho_s^2)(1+k_4^2\rho_s^2)} - \Delta_{42}\Delta_{23}\Delta_1\right)\phi_1 = 0 \tag{25}$$

where

$$\Gamma = (k_2^2 - k_1^2)\left(\frac{k_4^2 - k_2^2}{1 + k_4^2\rho_s^2} - \frac{k_2^2 - k_3^2}{1 + k_3^2\rho_s^2}\right) \qquad \Delta_1 = \frac{\boldsymbol{v}\cdot\boldsymbol{k}_1}{1 + k_1^2\rho_s^2} \qquad \Delta = \Delta_{42} - \Delta_{23}$$

and Δ_{23} and Δ_{42} are as defined in section 3.1.

Seeking solutions to equation (25) of the form $\phi_1(t) = \phi_1 e^{\lambda t}$ yields a cubic equation, which can be solved analytically for λ using the standard formula [16]. However, it is more illuminating to estimate the instability growth rate by using some approximations. It is easy to see that, for reasonable values of the various parameters ($\rho_s k_1 \ll 1$, $\rho_s k_{2,3,4} \leqslant 1$, $\rho_s/L_n \ll 1$), the term in equation (25) proportional to ϕ_1 is comparatively small and can be neglected. One thus obtains a quadratic equation for λ which, using the ordering given above, yields the following simplified expression for the streamer growth rate (real part of λ)

$$\gamma_S \simeq \frac{A'|\phi_2|\Gamma^{1/2}\rho_s^2}{\sqrt{1 + \rho_s^2 k_1^2}} \simeq A'|\phi_2|\Gamma^{1/2}\rho_s^2. \tag{26}$$

With the same approximation, the growth rate for zonal flows can be estimated from equation (18)

$$\gamma_Z \simeq A|\phi_2|\frac{\alpha^{1/2}}{k_1}. \tag{27}$$

Note that this approximation for γ_Z is the same as in equation (19), except that here we do *not* further approximate the factor α by assuming that terms proportional to $(k_2^2\rho_s^2)^2$ can be neglected. The ratio of the two approximate expressions for the streamer and zonal flow growth rates is

$$\frac{\gamma_S}{\gamma_Z} = \frac{\Gamma^{1/2}\rho_s^2 k_1}{\alpha^{1/2}} = \left(\frac{k_2^2\rho_s^2 - k_1^2\rho_s^2}{1 + k_2^2\rho_s^2 - k_1^2\rho_s^2}\right)^{1/2} \rho_s k_1 \ll 1. \tag{28}$$

It appears that the growth rate of streamers is considerably smaller than that of zonal flows. Zonal flows, therefore, tend to grow faster than streamers, within the model framework considered here. In a situation of fully developed turbulence, where energy is exchanged nonlinearly among a large number of modes, this may imply that zonal flows play a more important role than streamers.

Physically, the difference from the case of zonal flows is that, in the streamer scenario of figure 1(b), all wavevectors including the streamer itself have a finite component (k_x) parallel to the flux surface in the direction of the equilibrium poloidal diamagnetic drift. For such modes, the electron response is the standard adiabatic one, as in the HM equation, and therefore the modes are subject to the (stabilizing) effect of the electron pressure. Contrarily, zonal flows, being constant on a flux surface ($k_x = 0$), are not affected by the electron pressure, and behave effectively as an incompressible fluid. Their instability drive is therefore stronger.

4. Numerical results

A numerical code that solves the generalized HM equation has been implemented using a pseudo-spectral method, according to which the potential is expanded in a Fourier series. The linear part of the equation is then trivial when expressed in Fourier space, while the nonlinear terms are computed in real space by using a fast Fourier transform (FFT) algorithm. Periodic boundary conditions are assumed for both directions. The advantages of the pseudo-spectral technique are that: (a) it allows a direct comparison with the analytical results, which also rely on Fourier modes; (b) it is particularly efficient for treating turbulent mode coupling in

a simple geometry. In order to deal with genuine broad-spectrum turbulence, a de-aliasing technique would need to be implemented in the code. However, this is not necessary for the four-wave problems studied here, and no de-aliasing has been included at this stage. Finally, a viscous dissipation term has been added on the right-hand side of equation (2), although this is not necessary for the four-wave problems considered in this paper.

The time-stepping is performed with a leap-frog technique. This is second-order accurate and conservative (oscillations are undamped), but tends to decouple even and odd time-steps. In order to obviate this drawback, a predictor–corrector scheme is used at regular intervals (say, every 100 time-steps) instead of the leap-frog scheme. The predictor–corrector scheme is also second-order accurate, and couples subsequent time-steps. Within each scheme, the linear and nonlinear terms are treated separately by means of a splitting technique. This can be illustrated on a model equation

$$\frac{\partial W}{\partial t} = -\Omega W - N(W) \tag{29}$$

where $N(W)$ represents symbolically the nonlinear terms and ΩW the linear ones, including viscosity. The leap-frog scheme can thus be represented in three steps (all quantities are supposed to be known up to step n)

(i) $W^*_{n-1} = W_{n-1} \exp(-\Omega \Delta t)$,
(ii) $W^*_{n+1} = W^*_{n-1} - 2\Delta t\ N(W_n)$,
(iii) $W_{n+1} = W^*_{n+1} \exp(-\Omega \Delta t)$,

where the asterisks represent intermediate results, and do not denote complex conjugation. Similarly, the predictor–corrector scheme can be represented in four steps

(i) $W^*_n = W_n \exp(-\Omega \Delta t/2)$,
(ii) $W_{n+1/2} = W^*_n - \Delta t/2\ N(W^*_n)$,
(iii) $W^*_{n+1} = W^*_n - \Delta t\ N(W_{n+1/2})$,
(iv) $W_{n+1} = W^*_{n+1} \exp(-\Omega \Delta t/2)$.

In order to simulate the fully nonlinear four-wave problem, the code has been run setting all other modes to zero at every time-step. The code is initialized by setting the pump wave at a finite amplitude $|\phi_2|$, while the sidebands and the zonal flow (or streamer) are seeded with a small perturbation.

4.1. Zonal flows

The wavenumber of the pump wave is $\rho_s \boldsymbol{k}_2 = (0.07, 0.08)$ and the zonal flow $\rho_s \boldsymbol{k}_1 = (0.0, 0.01)$. Further, we take $L/L_n = 1$, where L and L_n are respectively the dimension of the domain and the scale length of the equilibrium plasma inhomogeneity. These values completely determine the two triads (figure 1). The criterion derived in the previous section states that instability occurs when the pump wave amplitude $|\phi_2|$ is larger than a certain threshold. Figure 2 shows the evolution of the zonal flow amplitude and a sideband in two cases where the criterion predicts instability[3]. An instability is indeed observed, and the analytical growth rates, represented by a straight line on the figures, are accurately reproduced in the simulation. We have verified numerically the threshold condition on the amplitude $|\phi_2|$, given in equation (17), which must be satisfied for linear instability.

[3] The initial condition in the simulations is a superposition of three normal modes with different real and imaginary frequencies. All normal modes influence the initial evolution, and linear growth emerges later in the simulations when the fastest growing mode has become dominant, i.e. for $t \gg 1/\gamma_Z$. This explains the apparently nonlinear behaviour observed early in the simulations in figures 2 and 3.

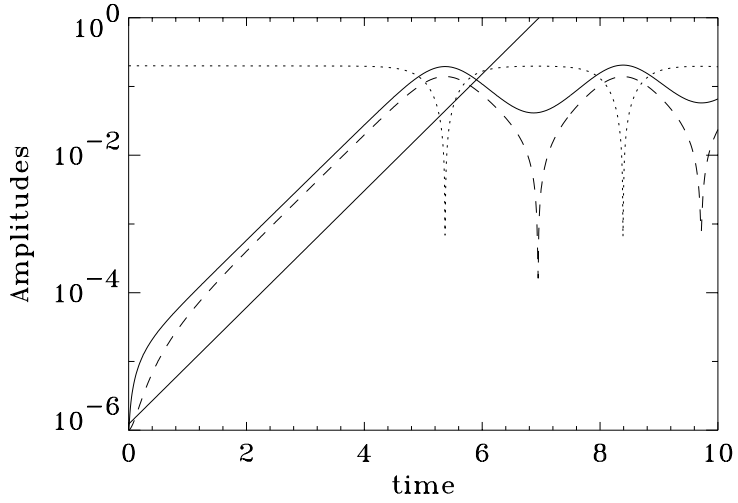

(a)

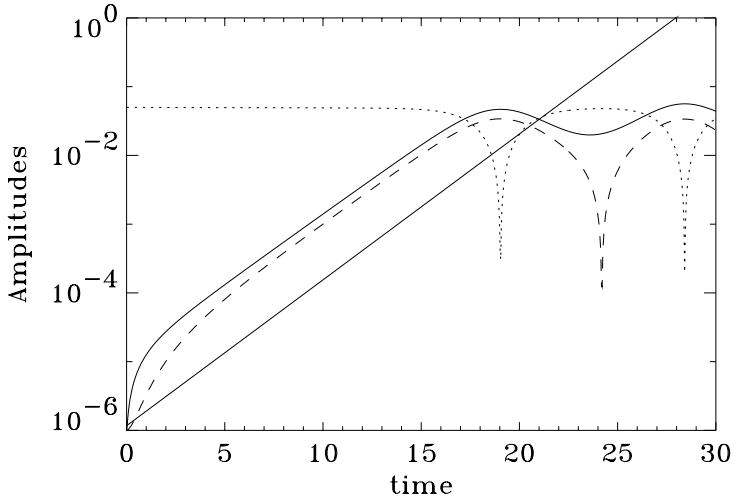

(b)

Figure 2. Time evolution of the zonal flow (full curve), pump wave (dotted curve) and sideband (dashed curve) amplitudes. The full straight line corresponds to the analytical growth rate from equation (18) ($\gamma \simeq 1.954$ for (a), $\gamma \simeq 0.489$ for (b)). The initial pump wave amplitude is $|\phi_2| = 0.2$ (a) and $|\phi_2| = 0.05$ (b). Time and amplitudes are in units of eBL^2/T_e and T_e respectively.

The simulations also show that the zonal flow saturates nonlinearly at an amplitude that is of the same order of magnitude as the initial pump wave amplitude. We stress, however, that the saturation mechanism observed here arises from a description which is incomplete and to that extent somewhat unphysical, being due to the nonlinear coupling of only four modes. In a fully turbulent (broad-band) simulation, nonlinear coupling to other modes would probably occur before the saturation observed in figures 2 and 3, thus affecting both the level and the time scale of real saturation. Note that these considerations apply to zonal flows as well as streamers. Nevertheless, it is interesting to investigate the nonlinear saturation mechanism

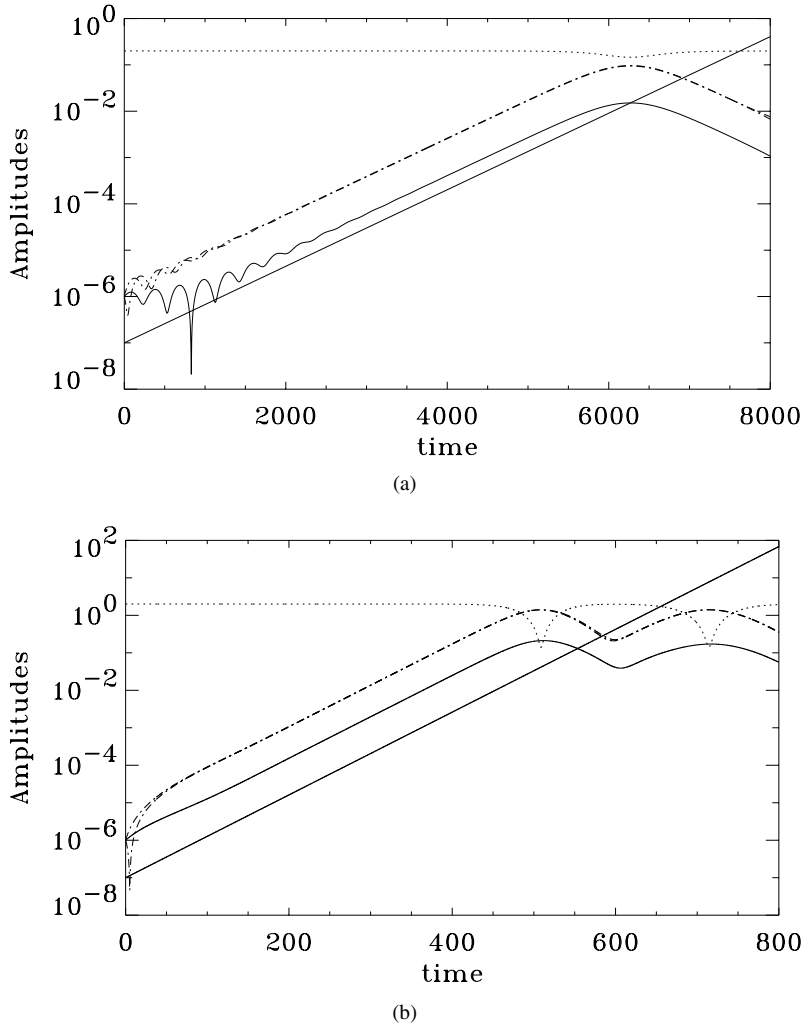

Figure 3. Time evolution of the streamer (full curve), pump wave (dotted curve) and sidebands (dash-dot curve) amplitudes. The full straight line corresponds to the analytical growth rate obtained from solving equation (25) ($\gamma \simeq 0.0019$ for (a), $\gamma \simeq 0.0254$ for (b)). The initial pump wave amplitude is $|\phi_2| = 0.2$ (a) and $|\phi_2| = 2$ (b). Time and amplitudes are in units of eBL^2/T_e and T_e respectively.

arising in the present four-wave model, both as a cross-check of the simulation results and a way to gain insight into the model. In order to do so, it is useful to employ the invariants defined in equations (7) and (8). We construct the following linear combinations of the invariants E and Z, for the four-wave problem considered here

$$I_1 = Z - \rho_s^2 k_1^2 E = (1+\rho_s^2 k_2^2)(1+\rho_s^2 k_2^2 - \rho_s^2 k_1^2)|\phi_2|^2 + (1+\rho_s^2 k_3^2)(1+\rho_s^2 k_3^2 - \rho_s^2 k_1^2)|\phi_3|^2 + (1+\rho_s^2 k_4^2)(1+\rho_s^2 k_4^2 - \rho_s^2 k_1^2)|\phi_4|^2 \quad (30)$$

$$I_2 = Z - (1+\rho_s^2 k_2^2)E = -\rho_s^2 k_1^2 (1+\rho_s^2 k_2^2 - \rho_s^2 k_1^2)|\phi_1|^2 + \rho_s^2 (1+\rho_s^2 k_3^2)(k_3^2 - k_2^2)|\phi_3|^2 - \rho_s^2 (1+\rho_s^2 k_4^2)(k_2^2 - k_4^2)|\phi_4|^2. \quad (31)$$

Notice that I_1 and I_2 only depend on *three* of the four waves involved in the problem. I_2 is independent of the pump wave ϕ_2, and its terms have different signs: therefore, each term can

grow arbitrarily large, as happens during the linear phase of the instability. The value of I_2 is small for the cases we treat and remains constant in time, which has been verified in the simulations (although numerical errors will be amplified, the range of variation of I_2 is still much smaller than that of each mode).

On the other hand, I_1 is positive definite and initially dominated by the pump wave. When the sidebands ϕ_3 and ϕ_4 have grown sufficiently large, it follows that the pump wave amplitude must necessarily decrease, in order to ensure the invariance of I_1. Saturation therefore occurs by depletion of the pump wave. Incidentally, this proves that no instability can occur if the pump wave is the zonal flow ϕ_1 itself: in that case, the three terms of I_1 could not all grow together, otherwise the invariance of I_1 would be violated. (The constancy of I_1 has been verified to high accuracy in the simulations).

The above arguments can be used to estimate the saturation level of the instability. Saturation occurs when the second and third terms of I_1 become comparable to the first. This yields an estimate for the saturation level of the sidebands

$$|\phi_{3,4}|^2 \simeq \frac{(1+\rho_s^2k_2^2)(1+\rho_s^2k_2^2-\rho_s^2k_1^2)}{(1+\rho_s^2k_{3,4}^2)(1+\rho_s^2k_{3,4}^2-\rho_s^2k_1^2)}|\phi_2|^2. \tag{32}$$

Inserting the parameters of the above simulations into this formula, we find that saturation should occur when $|\phi_{3,4}| \simeq |\phi_2|$, which is in fairly good agreement with the numerical results of figure 2. After saturation, the system enters a multiply periodic regime.

4.2. Streamers

For this set of simulations we have $\rho_s\boldsymbol{k}_2 = (0.07, 0.08)$ for the pump wave and $\rho_s\boldsymbol{k}_1 = (0.01, 0.0)$ for the streamer. Furthermore, we take $(L/L_n = 1)$, as in the zonal flow simulations of section 4.1. The analytical growth rate must therefore be found by solving the cubic equation associated to equation (25). Consistently with the estimation found previously (see equation (28)), the growth rate is extremely low for values of the pump wave amplitude similar to those used for the zonal flow runs reported above. When the amplitude is $|\phi_2| = 0.2$ (figure 3(a)), the growth rate is considerably lower than for zonal flows with the same pump wave amplitude (figure 2(a)) (note the different scales for the time axis), although the saturation level is similar. In order to observe significant growth rates, we had to use a much higher amplitude, such as $|\phi_2| = 2$ (figure 3(b)). Again, the saturation level is proportional to the initial pump wave amplitude.

Invariant quantities, based on the general energy and enstrophy invariants, can be found for the streamer case too, following the same procedure employed for zonal flows in section 4.1. Their analysis again indicates that saturation should occur when the sidebands reach a level comparable to that of the pump wave. As mentioned earlier, however, a proper estimate of saturation should include nonlinear couplings to all other modes (broad-band turbulence), which is likely to affect both the saturation level and time scale.

5. Conclusions

We have presented both analytical and numerical calculations of the growth of long wavelength zonal flows in the generalized HM system recently proposed by Smolyakov *et al* [11, 12]. We have performed an analytic calculation of the linear growth rate for a narrow-band four-wave problem. This is simpler, but also less general, than the treatment outlined in [11, 12], which was based on a wave kinetic equation. Making the same approximations as were assumed in [11, 12], we have obtained an analytic linear growth rate that appears to differ by a factor of $\sqrt{2}$ from that calculated in [12] using different methods. A spectral code has been developed

for studying the properties of this model system, and numerical computations for this four-wave problem show good agreement with our analytic result. In addition, the linear growth rate for streamer structures has also been calculated for a similar four-wave problem. This turns out to be much lower than the growth rate for zonal flows, at least in the limit of small Larmor radii. The analysis of the invariants for the four-wave system reveals that nonlinear saturation should occur via depletion of the pump wave, as is observed in the simulations.

The present results bear some resemblance to the well known literature on the nonlinear coupling of three drift waves [17–19]. However, our primary aim was to explore the results of Smolyakov *et al* [11, 12] in the weak turbulence limit. For a correct treatment of the weak turbulence problem, it was necessary to keep both sidebands, and thus utilize a four-wave model. This is supported by the fact that, if one of the sidebands is not initially excited (but left free to grow), it will still be driven by the instability. The results presented here thus make a connection between the WKB-type work of Smolyakov *et al* [11, 12], and the standard results on the interaction of three drift waves [17–19], extending them to the case of four waves.

Our spectral code is now well benchmarked against theory for the analytically tractable case of four-wave interaction. It will be interesting, in the future, to enhance this code for the study of fully-developed broad-band turbulence. For this purpose, the only missing computational ingredient is a de-aliasing scheme, which should be implemented in order to ensure the accuracy of the algorithm. The code will then constitute a reliable tool to simulate two-dimensional turbulence in some paradigm models of the HM type.

Zonal flow and streamer physics is, at present, a topical area of research (see, for instance, the recently published references [1, 2, 20]). The problem of zonal flow generation using a large-scale gyrokinetic code is addressed by [1]. The authors find that zonal flows can be excited by linear ITG modes by a mechanism similar to the Kelvin–Helmoltz instability, with rather large growth rates. Their model differs from ours in several important respects including (a) the ITG mode is linearly unstable, whereas our pump wave is stable; and (b) they consider small scale zonal flows, for which $\rho_s k_r \simeq 1$. However, when comparable sets of parameters and regimes are analysed, Rogers *et al* [1] find a growth rate qualitatively similar to ours. Finally, they identify the possibility that the zonal flow can itself be damped away by nonlinear instabilities. This 'tertiary' instability requires the presence of a temperature gradient, and is thus not applicable to our model.

Reference [20] is entirely devoted to a detailed statistical analysis of the generalized HM equation employed in the present paper. Numerical simulations of such a model have not been attempted to date, and would provide interesting information on the emergence and dynamics of global structures (such as zonal flows and streamers) in broad-band plasma turbulence. As the physical effects incorporated in our model constitute the core of many large-scale codes, the results could improve our understanding of some fundamental issues of plasma turbulence in a magnetized environment such as that of tokamaks.

In conclusion, the results presented in this paper provide *ab initio* information concerning the excitation and saturation of large-scale flows (both zonal flows and streamers) in magnetized plasmas. As test-particle transport, both radial [21] and poloidal [22], has been shown to be sensitive to the nature of the underlying turbulent fields, the effects described above may also have an impact on the confinement of charged particles in fusion devices.

Acknowledgments

The authors would like to acknowledge valuable contributions from useful discussions with J W Connor, P Bertrand, C N Lashmore-Davies and A Thyagaraja. This work was jointly funded by the UK Department of Trade and Industry and EURATOM, with additional support from EURATOM mobility funding.

References

[1] Rogers B N, Dorland W and Kotschenreuther M 2000 *Phys. Rev. Lett.* **85** 5336
[2] Beyer P, Benkadda S, Garbet X and Diamond P H 2000 *Phys. Rev. Lett.* **85** 4892
[3] Ottaviani M and Manfredi G 2001 *Nucl. Fusion* **41** 637
Ottaviani M and Manfredi G 1999 *Phys. Plasmas* **6** 3267
[4] Cohen B I, Williams T J, Dimits A M and Byers J A 1993 *Phys. Fluids* B **5** 2967
[5] Parker S E, Dorland W, Santoro R A, Beer M A, Liu Q P, Lee W W and Hammett G W 1994 *Phys. Plasmas* **1** 1461
[6] Dimits A, Williams T J, Byers J A and Cohen B I 1996 *Phys. Rev. Lett.* **77** 71
[7] Lin Z, Hahm T S, Lee W W, Tang W M and White R B 1998 *Science* **281** 1835
[8] Hasegawa A and Mima K 1978 *Phys. Fluids* **21** 87
[9] Horton W and Hasegawa A 1994 *Chaos* **4** 227
[10] Manfredi G 1999 *J. Plasma Phys.* **61** 601
[11] Smolyakov A I, Diamond P H and Malkov M 2000 *Phys. Rev. Lett.* **84** 491
[12] Smolyakov A I, Diamond P H and Shevchenko A I 2000 *Phys. Plasmas* **7** 1349
[13] Chen L, Lin Z and White R 2000 *Phys. Plasmas* **7** 3129
[14] Guzdar P N, Kleva R G and Chen L 2001 *Phys. Plasmas* **8** 459
[15] Dendy R O and ter Haar D 1984 *J. Plasma Phys.* **31** 67
[16] Abramowitz M and Stegun I A 1970 *Handbook of Mathematical Functions* (New York: Dover) p 17
[17] Terry P W and Horton W 1982 *Phys. Fluids* **25** 491
[18] Waltz R E 1983 *Phys. Fluids* **26** 169
[19] He K and Biskamp D 1985 *Phys. Lett.* A **108** 347
[20] Krommes J A and Kim C-B 2000 *Phys. Rev.* E **62** 8508
[21] Manfredi G and Dendy R O 1997 *Phys. Plasmas* **4** 628
Manfredi G and Dendy R O 1996 *Phys. Rev. Lett.* **76** 4360
[22] Annibaldi S V, Manfredi G, Dendy R O and Drury L O'C 2000 *Plasma Phys. Control. Fusion* **42** L13